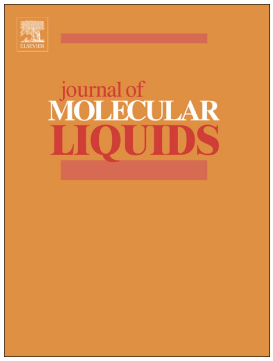

Molecular interactions between 1-butyl-3-methylimidazolium tetrafluoroborate and model naphthenic acids: A DFT study

Chongchong Wu, Alex De Visscher, Ian D. Gates

PII: S0167-7322(17)32649-1
DOI: doi: 10.1016/j.molliq.2017.08.061
Reference: MOLLIQ 7769

To appear in: *Journal of Molecular Liquids*

Received date: 17 June 2017
Revised date: 11 August 2017
Accepted date: 14 August 2017

Please cite this article as: Chongchong Wu, Alex De Visscher, Ian D. Gates , Molecular interactions between 1-butyl-3-methylimidazolium tetrafluoroborate and model naphthenic acids: A DFT study, *Journal of Molecular Liquids* (2017), doi: 10.1016/j.molliq.2017.08.061

Molecular Interactions between 1-Butyl-3-methylimidazolium Tetrafluoroborate and Model Naphthenic Acids: A DFT Study

Chongchong Wu[a], Alex De Visscher[a, b], Ian D. Gates[a*]

[a]Department of Chemical and Petroleum Engineering, University of Calgary, Alberta, Canada
[b]Department of Chemical and Materials Engineering, Concordia University, Montreal, Quebec, Canada

Abstract

A density functional theory study was performed to investigate the interactions between 1-butyl-3-methylimidazolium tetrafluoroborate ([BMIM][BF_4]) and six different model naphthenic acids (NAs). Natural bond orbital, atoms in molecules, noncovalent interactions, HOMO-LUMO overlap integral, and electron density difference were analyzed. The analysis informs on the use of ionic liquids as solvents for the removal of NAs from crude oil. The main extraction mechanism for NAs without long alkyl chain is hydrogen bonding, whereas van der Waals interaction and hydrogen bonding are the dominant extraction mechanisms for NAs with long alkyl chain. F···H hydrogen bonding is the strongest hydrogen bond, and O···H is the second strongest for all the interactions. NAs with polycyclic hydrocarbons or multiple carboxylic groups have larger total interaction energies than those with monocyclic hydrocarbons and one carboxylic group. The results indicate that σ(C-O)-σ*(C-H), LP(O)-σ*(C-H), σ*(C-O)-σ*(C-H), and σ(C-H)-σ*(C-O) interactions can occur between [BMIM][BF_4] and model NAs without aromatic ring, whereas π(C-O)-σ*(C-H), LP(O)-σ*(C-H), π*(C-O)-σ*(C-H), and σ(C-H)-π*(C-O) interactions take place for [BMIM][BF_4]-benzoic acid.

Key words: Naphthenic acids; ionic liquids; density functional theory**;** 1-butyl-3-methylimidazolium tetrafluoroborate; extraction mechanism

*Corresponding Author: Ian Gates
Phone: +1-403-220-5752
Email: ian.gates@ucalgary.ca

Abbreviations:

NAs	naphthenic acids
ILs	ionic liquids
[BMIM][BF_4]	1-butyl-3-methylimidazolium tetrafluoroborate
CHCA	cyclohexanecarboxylic acid
CPCA	cyclopentanecarboxylic acid
BA	benzoic acid
CHPA	cyclohexanepentanoic acid
CHDCA	1,4-cyclohexanedicarboxylic acid
DCHA	dicyclohexylacetic acid
NBO	natural bond orbital
HOMO	highest occupied molecular orbital
LUMO	lowest unoccupied molecular orbital
NCI	noncovalent interactions
AIM	Atoms in molecules
VDW	van der Waals
BCP	bond critical point

1. Introduction

Naphthenic acids (NAs), a mixture of alkyl-substituted cyclic aliphatic carboxylic acids, are among the most common oxygen-containing compounds in crude oil [1, 2]. The presence of NAs increases the acidity of crude oils, and causes serious corrosion to oil refining equipment, transportation pipelines, and storage tanks [3]. NAs also induce other serious problems such as poisoning catalysis, forming coke, and emulsions [4]. Therefore, it is important to remove NAs from crude oil and NAs removal is critical for heavy oil upgrading [5]. Several methods are used to separate NAs from crude oil including aqueous solution washing, solvent extraction, adsorption, catalytic esterification, and decarboxylation [6], but these methods have their drawbacks, making it critical to investigate alternative approaches to remove NAs from crude oil.

Ionic liquids (ILs) are nonvolatile, thermally stable, nonflammable, and environmentally friendly green solvents, and they are considered favorable solvents for many separation processes [7, 8]. Recently, significant progress has been made to utilize ILs to separate NAs from crude oil. Anderson et al. used tetraalkylammonium and tetraalkylphosphonium amino acid-based ILs to remove NAs from crude oil [9]. Sun et al. attempted to use imidazole anion and 1-alkyl-3-methylimidazolium imidazolide to separate NAs from crude oil [10]. Shah et al. investigated the isolation of NAs from highly acidic model oil using imidazolium-based ILs and hydroxide-based ILs [11, 12]. In addition, the separation of NAs from crude oil was also realized through employing thiocyanate-based ILs [13].

Considering the structures and diversity of functionalities of ILs, most types of interactions, including dispersive, π-π, n-π, hydrogen bonding, dipolar, and ionic/charge-charge, can occur between ILs and other compounds [14]. Moreover, the composition of NAs are often complex and therefore, the interactions between ILs and NAs are different based on the structures of NAs.

Although it is difficult and time-consuming to investigate IL-based extraction mechanisms for NAs through experiment, the interactions of ILs and compounds can be explored through quantum chemical computation [15, 16]. Despite the numerous experimental investigations on the application of ILs to separate NAs from crude oil [9-13], few detailed computational studies have been reported on the direct interactions between ILs and NAs thus far. Furthermore, current theoretical studies mainly focus on IL-based extraction of sulfur and nitrogen-containing compounds from fuels [17-19]. Due to structural differences between NAs and sulfur and nitrogen-containing compounds, it is necessary to investigate the ILs extraction mechanisms of NAs to instruct the design of ILs for efficient NAs removal.

Here, we fill the gap by examining mechanistic interactions between ILs and six model NAs by using density functional theory. More specifically, we examine the extraction mechanism between 1-butyl-3-methylimidazolium tetrafluoroborate ([BMIM][BF_4]) as a model IL and cyclohexanecarboxylic acid (CHCA), cyclopentanecarboxylic acid (CPCA), benzoic acid (BA), cyclohexanepentanoic acid (CHPA), 1,4-cyclohexanedicarboxylic acid (CHDCA), and dicyclohexylacetic acid (DCHA) as model NAs. BA is not strictly a NA, but the six compounds will be categorized collectively as NAs for convenience. The electronic structures, interaction energies, and the intermolecular interactions including van der Waals interactions, hydrogen bonds, and electrostatic interactions, were analyzed. The structures for [BMIM][BF_4] and six types of model NAs are shown in Fig. 1.

2. Computational Methods

The density functional computations were performed by using the Gaussian 09 program package [20]. Many theoretical studies on ILs were carried out by using M06-2X/6-311++g(d,p) level of theory [21-25]. Therefore, the structures of [BMIM][BF_4] and the six different model

NAs were optimized by using the M06-2X method and 6-311++G(d,p) basis set. The [BMIM][BF_4]-model NAs structures were also optimized by using the same method and basis set. The interaction energies were calculated at M06-2X/6-311++G(d,p) level with the correction by the basis set superposition error method. The second-order perturbation energy $E(2)$ in the natural bond orbital (NBO) was investigated in Gaussian 09 at the M06-2X/6-311++G(d,p) level of theory. The highest occupied molecular orbital (HOMO) and lowest unoccupied molecular orbital (LUMO) were calculated. Analyses of the noncovalent interactions (NCI) and electron density difference were carried out by analyzing the wave functions for the optimized structures using the Multiwfn software package [26, 27]. The coulomb-attenuating method CAM-B3LYP, which considers long-range interactions, was used in combination with 6-311++G(d,p) basis set to perform HOMO-LUMO overlap integral analysis [28]. Topological properties were analyzed by using atoms in molecules (AIM) theory [29].

3. Results and Discussion

3.1. Optimized geometries

After optimization of $[BMIM]^+$ and $[BF_4]^-$, $[BF_4]^-$ was positioned at different orientations around $[BMIM]^+$, and those structures were optimized to determine the most stable cation-anion pair of [BMIM][BF_4]. Also, the structures of six types of model NAs were optimized, and electrostatic potential analysis was conducted; the results are displayed in Fig. 2. It was observed that $[BF_4]^-$ has a strongly negative electrostatic potential, whereas $[BMIM]^+$ has a high positive electrostatic potential. Regarding the six types of model NAs, the most negative electrostatic potentials are located around the oxygen atoms in the carboxylic groups, and the most positive electrostatic potentials are located around the hydrogen atoms in the carboxylic groups. To obtain the most stable geometries for the interactions between [BMIM][BF_4] and model NAs,

model NAs were placed in different regions around the optimized [BMIM][BF_4] to form complexes according to electrostatic potential analysis. Then, different structures were optimized, and the most stable geometry was the structure with the lowest energy and without imaginary frequency.

The most stable molecular structures for [BMIM][BF_4] and [BMIM][BF_4]-model NAs are shown in Fig. 3 with Cartesian co-ordinates summarized in Table S1. It was noted that the most stable geometry for [BMIM][BF_4] calculated with the 6-311++G(d,p) basis set (Fig. 3a) varies from the geometry calculated with the 6-311G(d,p) basis set (Fig. 3b). Additionally, the energy deviation between the two structures is 9.95 kcal/mol. With the addition of two diffusion functions, the 6-311++G(d,p) basis set can better represent the electron distributions [30], hence, it was chosen for the current study. The van der Waals (VDW) radii for fluorine and hydrogen are 1.2 and 1.47 Å, respectively [31]. Therefore, several hydrogen bonds are formed between the hydrogen atoms in the cation and fluorine atoms in the anion of [BMIM][BF_4], shown in Fig. 3a. The hydrogen bond distances between H13 and F30, H13 and F26 are shorter than the hydrogen bond lengths formed by other hydrogen atoms (H18, H19) owing to the high electron potential of H13. H18 is closer to the imidazole ring than H19, consequently, the H18…F26 hydrogen bond is shorter than H19⋯F26. In addition, the interactions between F28 and C5 in the imidazole ring indicates the existence of lone pair (LP)-π interactions in [BMIM][BF_4].

After forming complexes with model NAs, the cation and anion in [BMIM][BF_4] form two prominent hydrogen bonds with model NAs: one is between the fluorine atom of $[BF_4]^-$ and the hydrogen atom in the carboxylic group of the model NAs and the other is between the hydrogen atom in $[BMIM]^+$ and the oxygen atom in the carboxylic group of the model NAs. The F51⋯H21 bond is shorter than the O19⋯H34 one, suggesting that the hydrogen bond between

the fluorine atom and hydrogen atom is stronger, displayed in Fig. 3c. It is noted that the F51⋯H34 bond length is longer after forming complexes because F51⋯H21 and H34⋯O19 hydrogen bond formation result in an increase of the F51 electrostatic potential and a decrease of the H34 electrostatic potential. Hence, the F51⋯H34 bond length is longer and the interaction is weaker (see Fig. 3c and Fig. 4), in agreement with the principle of bond order conservation. Meanwhile, the formation of the F51⋯H21 and H34⋯O19 hydrogen bonds causes the F49⋯C26, F49⋯H40, and F47⋯H39 bonds to elongate, suggesting that the interactions between $[BF_4]^-$ and $[BMIM]^+$ are weaker (see Fig. 3c). Interestingly, O19 and H21 in the carboxylic group form an intermolecular hydrogen bond in [BMIM][BF_4]-CHCA. The interaction between [BMIM][BF_4] and other five types of NAs follow the same trends as [BMIM][BF_4]-CHCA. For the electrostatic potential, the highest negative values are located around the interaction region between [BMIM][BF_4] and model NAs, whereas the largest positive values are located around the hydrogen atoms in the imidazolium ring, as shown in Fig. 4.

3.2. Interaction energies

Interaction energies between [BMIM][BF_4] and model NAs can help to evaluate the stability of complexes, and moreover help to explain the different extraction efficiencies for NA extraction. The interaction energies were calculated according to Eq. (1):

$$\Delta E = \left(E_{[BMIM]][BF_4]} + E_{Model\ NAs}\right) - E_{[BMIM][BF_4]-Model\ NAs} \quad (1)$$

The interaction energies between [BMIM][BF_4] and CHCA/CPCA/BA/CHPA/CHDCA/DCHA are 15.22, 15.07, 15.63, 14.34, 16.36, and 16.57 kcal/mol, respectively.The interaction energy for [BMIM][BF_4]-DCHA is highest with [BMIM][BF4]-CHDCA ranking second among the

interactions between [BMIM][BF_4] and six types of model NAs, therefore, it was deduced that the interaction energy between [BMIM][BF_4] and NAs with two cyclohexane rings is larger than that with one, and the interaction energy for NAs with two carboxylic groups is larger than that with one carboxylic group. In addition, it is expected that the second carboxylic group in CHDCA is capable of forming complexes with a second [BMIM][BF_4] molecule, which will result in higher interaction energy. Accordingly, [BMIM][BF_4] is more favorable to extract NAs with polycyclic hydrocarbons or multiple carboxylic groups.

3.3. NBO analyses

To obtain donor-acceptor interactions between [BMIM] and model NAs, NBO analysis and a second-order perturbation theory analysis were carried out. The results are listed in Table S2. According to the results, there are four kinds of donor-acceptor interactions for stable hydrogen bonds between CHCA/CPCA/CHPA/CHDCA/DCHA and $[BMIM]^+$: σ(C-O)-σ*(C-H), LP(O)-σ*(C-H), σ*(C-O)-σ*(C-H), and σ(C-H)-σ*(C-O). In addition, π(C-O)-σ*(C-H), LP(O)-σ*(C-H), π*(C-O)-σ*(C-H), and σ(C-H)-π*(C-O) interactions exist between BA and $[BMIM]^+$. With regards to the interactions between CHCA/CPCA/ CHPA/CHDCA/DCHA and $[BF_4]^-$, there are two main kinds of hydrogen bonding interactions: σ(O-H)-σ*(B-F) and LP(F)-σ(O-H). On the other hand, only the LP(F)-σ(O-H) interaction takes place between BA and $[BF_4]^-$. The remarkable difference can be ascribed to the reason that BA has an aromatic ring and the other five types of NAs are nonaromatic. Interestingly, the stabilization energy E(2) of LP(F)-σ(O-H) and LP(O)-σ*(C-H) is substantially greater than that of the other interactions, exhibiting that LP(F)-σ(O-H) and LP(O)-σ*(C-H) interactions are stronger. In addition, the stabilization energy

E(2) for LP(F)-σ(O-H) is larger than that of LP(O)-σ*(C-H). NBO analysis results are consistent with the findings from the geometry analysis.

The charge distributions of [BMIM][BF_4], model NAs, and [BMIM][BF_4]-NAs were summarized in Table S3. For isolated model NAs, the hydrogen atom with the highest NBO charge is H21(0.48598), H18(0.48847), H15(0.49089), H33(0.48608), H24(0.48743), and H40(0.48313) in CHCA, CPCA, BA, CHPA, CHDCA, and DCHA, respectively, which is attributed to the electronegativity of oxygen atom in the carboxylic group. After being absorbed by [BMIM][BF_4], LP(F)-σ(O-H) interactions between [BMIM][BF_4] and CHCA/CPCA/BA/CHPA/DCHA, lead to a more negative charge of the fluorine atom in $[BF_4]^-$ and more positive charge for hydrogen atoms in model NAs. Similarly, LP(O)-σ*(C-H) interactions give rise to the decrease of charge for oxygen atom in the carboxylic group of model NAs and increase of charge for intereracting hydrogen atoms in $[BMIM]^+$. Consequently, it is deduced that the complex formation, especially the strong hydrogen bond formation, results in the charge redistribution.

The σ, π occupancy and linear combination of some natural atomic orbitals of $[BMIM]^+$ in isolated [BMIM][BF_4], and [BMIM][BF_4]-NAs were exhibited in Table S4 to investigate the influence of interactions on the orbital formation of the cation. The hybridization of N1, C2, C3, and N4 atoms in σ(N1-C2), σ(N1-C5), σ(C2-C3), σ(C3-N4), and σ(N4-C5) are essentially the same after adsorbing model NAs, whereas the hybridization of C5 atom in the imidazole ring shows a clear deviation. As for the hybridization of σ(C5-H13), σ(C6-H14), and σ(C7-H18), it is noted that there are huge differences for C5(C26) and C6(C27) atoms after [BMIM][BF_4] interacts with CHCA, changing from $sp^{1.60}$ to $sp^{1.53}$, and $sp^{2.88}$ to $sp^{2.79}$, respectively, whereas the the hybridization of C7(C28) atom roughly remain the same. According to the geometry and

donor-acceptor interactions analysis, LP(O19)-σ*(C26-H34)/σ*(C27-H35), σ(C18-O19)-σ*(C26-H34)/σ*(C27-H35), σ*(C18-O19)-σ*(C26-H34)/σ*(C27-H35), and σ(C6-C18)-σ*(C26-H34) interactions could account for the hybridization changes of C26(C5) and C27(C6) atoms for [BMIM][BF_4]-CHCA. On the other hand, no strong interactions are formed for the C28(C7) atom, therefore, its hybridization practically maintain the same. The hybridization changes of σ(C5-H13), σ(C6-H14), and σ(C7-H18) for [BMIM][BF_4]-CPCA/BA follow the same trends as [BMIM][BF_4]-CHCA. However, C5 and C7 atoms in [BMIM][BF_4]-CHPA/CHDCA go through notable hybridization variation while hybridization of C6 atom virtually keeps unchanged. As for [BMIM][BF_4]-DCHA, only the C5 atom experiences significant hybridization alteration, compatible with geometry and donor-acceptor interactions analysis.

3.4. The topological properties of interactions

Atoms in molecules (AIM) analysis was performed to investigate the topological properties of interactions [29]. The total electronic density ρ(r) and Laplacian $\nabla^2\rho(r)$ at the bond critical point (BCP) are useful to illustrate the characteristics of the chemical bonds. The results are displayed in Fig. S1 and listed in Table. S5. The results show that [BMIM][BF_4]-CHCA, [BMIM][BF_4]-CPCA, and [BMIM][BF_4]-BA have 10 BCPs, whereas [BMIM][BF_4]-CHPA, [BMIM][BF_4]-CHDCA, [BMIM][BF_4]-DCHA have 15, 17, and 19 BCPs, respectively. The greater the alkyl chain length, number of carboxylic groups, and number of cyclohexane rings, the greater the opportunity for hydrogen-hydrogen (VDW) interactions as well as hydrogen bonding formation between model NAs and $[BMIM]^+$, resulting in more BCPs.

The electron density ρ(r) of BCPs represents the strength of interactions; larger value means a stronger interaction [32, 33]. According to Table. S5, the F51⋯H21 interaction has the largest ρ(r) and the O19⋯H34 bond ranks second for [BMIM][BF_4]-CHCA, implying that the F51-H21 and O19-H34 interactions are stronger than other interactions. Due to the larger electronegativity of fluorine than oxygen, F-H interaction is stronger than O-H interaction. Moreover, [BMIM][BF_4]-CPCA, [BMIM][BF_4]-BA, [BMIM][BF_4]-CHDCA, and [BMIM][BF_4]-DCHA also follow the same trends as [BMIM][BF_4]-CHCA. In summary, ρ(r) is greatest for interactions between the hydrogen atom (in the carboxylic group) and the fluorine atom (closest to that hydrogen atom), and is second largest for the interactions between the oxygen atom (connecting with carbon through double bond in the carboxylic group) and the hydrogen atom in $[BMIM]^+$ (closest to that oxygen atom). Nevertheless, the strongest interaction for [BMIM][BF_4]-CHPA is the H54⋯H22 bond. Therefore, it is concluded that hydrogen bonding is the main interaction for NAs without long alkyl chains, whereas VDW and hydrogen bonds interactions are the main interactions for NAs with long alkyl chains. The hydrogen bonding extraction mechanism was confirmed by Shah et al. in their experimental study [12]. It is also consistent to the mechanism proposed by Anderson et al. [9]. The value of the Laplacian of the electron density is positive for interactions between [BMIM][BF_4] and the six model NAs. This means that the electrons tends to segregate. The positive value also demonstrates that ionic bonds, hydrogen bonds, and VDW interactions exist in the six complexes formed between [BMIM][BF_4] and model NAs [34].

3.5. NCI analyses

NCI analyses can provide information about intramolecular and intermolecular interactions to distinguish interaction types and strength [35]. To investigate interaction types and strength,

the plots of reduced density gradient (RDG) versus sign(λ_2)ρ, and the gradient isosurface (s=0.7 a.u.) for [BMIM][BF_4] and [BMIM][BF_4]-model NAs are displayed in Fig. 5. In the left figure, the peaks at the sign(λ_2)$\cdot\rho$<0 region suggests attractive interactions such as hydrogen bond interactions and π-π interactions, whereas the spikes close to sign(λ_2)$\cdot\rho$=0 exhibit VDW interactions. On the other hand, peaks at the sign(λ_2)$\cdot\rho$>0 region indicate steric effects. In the gradient isosurface figure, the interaction types and strength can be identified through analyzing the color and area.

As shown in Fig. 5a, There is no peak in the hydrogen bond region of [BMIM][BF_4], demonstrating no apparent hydrogen bonds in [BMIM][BF_4]. As for complexes formed between [BMIM][BF_4] and model NAs, the spikes at -0.04 a.u. as well as the dark blue circle between the hydrogen atom and fluorine atom in the gradient isosurface figure indicate the existence of strong hydrogen bonding, as shown in Figs. 5b, 5c, and 5d. The spikes at -0.04 a.u. correspond to the strong fluorine and hydrogen interactions according to electron density analysis (see Table. S5). On the contrary, there is no spike at -0.04 a.u. in Figs. 5e, 5f, and 5g, suggesting that the hydrogen bonds at -0.04 a.u between [BMIM] and CHPA/CHDCA/DCHA are weaker. Moreover, the existence of peaks at -0.02 a.u. relates to hydrogen bonds formed between the oxygen atom in the model NAs and hydrogen atom in [BMIM][BF_4]. It is noteworthy that an oxygen atom can form several hydrogen bonds with hydrogen atoms in the ILs. The F-H hydrogen bond is stronger than O-H hydrogen bonds, hence, the hydrogen bonds formed between the anion and model NAs is stronger than that formed between the cation and model NAs.

The area and color between the anion and cation in the [BMIM][BF_4] are essentially the same after forming interactions with model NAs. It was deduced that the intramolecular LP-π interactions formed between the anion and cation in [BMIM][BF_4] are not destroyed by the

interactions with model NAs. Furthermore, due to the long alkyl chain of CHPA, the hydrogen atoms on the alkyl chain can form VDW interactions with [BMIM][BF_4], as indicated by the peaks around 0.00 a.u. as shown in Fig. 5e.

3.6. The HOMO-LUMO overlap integral analyses

It is reported that overlap of the molecular orbitals occurs when ILs interact with compounds, and orbital overlap analysis is beneficial to understand the interactions [36, 37]. In this section, we explored the HOMO and LUMO orbitals of [BMIM][BF_4] and model NAs, with results displayed in Fig. 6, as well as the HOMO-LUMO and LUMO-HOMO integrals between [BMIM][BF_4] and model NAs, with results shown in Fig. S2. A positive overlap integral indicates the attraction of two molecular orbitals whereas a negative value means repulsion of molecular orbitals.

The results reveal that HOMO of CHCA, CPCA, CHPA, CHDCA, and DCHA have a four-leaf clover shape orbital near the carboxylic group. In addition, the LUMO of CHCA, CPCA, CHPA, CHDCA, and DCHA occupy a large space near the hydrogen atom of the carboxylic group. On the other hand, neither the four-leaf clover shape nor large area are found for the HOMO and LUMO of BA, as shown in Fig. 6. The overlap integral between HOMO of [BMIM][BF_4] and LUMO of CHPA/CHDCA is negative, whereas the overlap integral between LUMO of [BMIM][BF_4] and HOMO of CHPA/CHDCA is positive, suggesting that LUMO-HOMO interactions are beneficial to [BMIM][BF_4]-CHPA/CHDCA complex formation. Furthermore, the overlap integral between HOMO of [BMIM][BF_4] and LUMO of CHCA/CPCA, and between LUMO of [BMIM][BF_4] and HOMO of CHCA/CPCA are both positive, indicating that both HOMO-LUMO and LUMO-HOMO interactions are beneficial to [BMIM][BF_4] and CHCA/CPCA interaction. On the other hand, the overlap integral between

HOMO of [BMIM][BF_4] and LUMO of BA/ DCHA are positive, and the overlap integral between LUMO of [BMIM][BF_4] and HOMO of BA/ /DCHA are negative, demonstrating that HOMO-LUMO is conducive to the interactions between [BMIM][BF_4] and BA/DCHA.

3.7. Electron density difference analysis

The formation of complexes between ILs and compounds generates electron density redistribution [38]. To understand the electron redistribution caused by the interaction between [BMIM][BF_4] and the six model NAs, electron density distribution maps were plotted shown in Fig. S3. The electron density change was calculated according to Eq. (2):

$$\Delta\rho = \rho_{[BMIM][BF_4]-Model\ NAs} - (\rho_{[BMIM][BF_4)} + \rho_{Model\ NAs}) \quad (2)$$

According to the results in Fig. S3, the difference of the electron density is located in the interaction region between IL and model NAs. The results reveal that the electron density of the carbon atom in the carboxylic group of model NAs is decreased. The reason is because of electron transfer from the carbon atom to the two adjacent oxygen atoms. Furthermore, the electron density of the oxygen atom connected with the carbon atom through double bond in the carboxylic group, is denoted purple in the exterior and green in the interior for all the six complexes, indicating the increase of electron density in the exterior of the complex and decrease in the interior of the complex. The explanation is due to the formation of hydrogen bonds between the oxygen atom and the hydrogen in [BMIM][BF_4] molecule leading to electron transfer from the interior of the complex to the exterior. Interestingly, the electron density of the oxygen atom connected with the hydrogen atom in the carboxylic group transfers from the center to the edges, induced by the redistribution of electrons during complex formation. Moreover,

electron transfers from the hydrogen atom in the carboxylic group to the adjacent oxygen atom give rise to the decrease of electron density in the hydrogen atom.

Due to the hydrogen bonding formation between [BMIM][BF_4] and model NAs, there are significant decreases of the electron density for hydrogen atoms both in [BMIM][BF_4] and model NAs. On the other hand, the electron transfer from those hydrogen atoms in the cation to the adjacent carbons causes the rise of the electron density between the carbon and hydrogen atoms. After hydrogen bond formation between one of the fluorine atoms in [BMIM][BF_4] and a hydrogen atom in model NAs, the electron densities of the participating fluorine atoms is raised, whereas the electron density between the fluorine atom and the boron atom is reduced, since electrons in that region are transferred to the neighboring fluorine atom, consistent with the principle of bond order conservation.

Overall, the electron density changes remarkably near the anion and carboxylic group for all six interactions, which is caused by the stronger hydrogen bonds of F⋯H and O⋯H. Compared with [BMIM][BF_4]-CHCA, [BMIM][BF_4]-CPCA, and [BMIM][BF_4]-BA, the hydrogen atoms in [BMIM][BF_4]-CHPA, [BMIM][BF_4]-CHDCA, and [BMIM][BF_4]-DCHA have pronounced electron density changes due to VDW interactions of hydrogen atoms. The results are consistent to the AIM analysis.

4. Conclusions

The interactions between [BMIM][BF_4] and CHCA/CPCA/BA/CHPA/CHDCA/DCHA were investigated by using the density functional theory approach. For NAs without a long alkyl chain, the main extraction mechanism is hydrogen bonding; For NAs with long alkyl chain, VDW interaction and hydrogen bonding are the dominant extraction mechanisms. [BMIM][BF_4] is more efficient at extracting NAs with polycyclic hydrocarbons or multiple carboxylic groups.

The bond characteristics and HOMO, LUMO orbitals for BA are different from the model NAs without aromatic ring. The LP-π interactions between $[BMIM]^+$ and $[BF_4]^-$ are not destroyed by the adsorption of model NAs on $[BMIM][BF_4]$, whereas the electron density changes remarkably near $[BF_4]^-$ and carboxylic group upon complexes formation. The study on the interactions between $[BMIM][BF_4]$ and six model NAs provide a comprehensive understanding of extraction mechanism by ILs, and will be beneficial for ILs design.

Acknowledgement

The financial support for the study provided by the Department of Chemical and Petroleum Engineering, University of Calgary, is acknowledged. The authors also acknowledge simulation support from Westgrid.

References

[1] P.J. Quinlan, K.C. Tam, Water treatment technologies for the remediation of naphthenic acids in oil sands process-affected water, Chem. Eng. J. 279 (2015) 696–714.

[2] C. Wu, A. De Visscher, I.D. Gates, Reactions of hydroxyl radicals with benzoic acid and benzoate, RSC Adv. 7 (2017) 35776–35785.

[3] M.K. Khan, A. Riaz, M. Yi, J. Kim, Removal of naphthenic acids from high acid crude via esterification with methanol, Fuel Process. Technol. 165 (2017) 123–130.

[4] K.A.P. Colati, G.P. Dalmaschio, E.V.R. De Castro, A.O. Gomes, B.G. Vaz, W. Romão, Monitoring the liquid/liquid extraction of naphthenic acids in brazilian crude oil using electrospray ionization FT-ICR mass spectrometry (ESI FT-ICR MS), Fuel. 108 (2013) 647–655.

[5] A. Zhang, Q. Ma, K. Wang, X. Liu, P. Shuler, Y. Tang, Naphthenic acid removal from crude oil through catalytic decarboxylation on magnesium oxide, Appl. Catal. A Gen. 303 (2006) 103–109.

[6] S. N. Shah, L. Kallidanthiyil Chellappan, G. Gonfa, M.I.A. Mutalib, R.B.M. Pilus, M.A. Bustam, Extraction of naphthenic acid from highly acidic oil using phenolate based ionic liquids, Chem. Eng. J. 284 (2016) 487–493.

[7] J. Lin, R. Lü, C. Wu, Y. Xiao, F. Liang, T. Famakinwa, A density functional theory study on the interactions between dibenzothiophene and tetrafluoroborate-based ionic liquids, J. Mol. Model. 23 (2017).

[8] R.A. El-Nagar, M. Nessim, A. Abd El-Wahab, R. Ibrahim, S. Faramawy, Investigating the efficiency of newly prepared imidazolium ionic liquids for carbon dioxide removal from natural gas, J. Mol. Liq. 237 (2017) 484–489.

[9] K. Anderson, P. Goodrich, C. Hardacre, A. Hussain, D.W. Rooney, D. Wassell, Removal of naphthenic acids from crude oil using amino acid ionic liquids, Fuel. 108 (2013) 715–722.

[10] Y. Sun, L. Shi, Basic ionic liquids with imidazole anion: New reagents to remove naphthenic acids from crude oil with high total acid number, Fuel. 99 (2012) 83–87.

[11] S.N. Shah, M.I.A. Mutalib, M.F. Ismail, H. Suleman, K.C. Lethesh, R.B.M. Pilus, Thermodynamic modelling of liquid-liquid extraction of naphthenic acid from dodecane using imidazolium based phenolate ionic liquids, J. Mol. Liq. 219 (2016) 513–525.

[12] S. N. Shah, M. I. A. Mutalib, R. B. M. Pilus, K. C. Lethesh, Extraction of naphthenic acid from highly acidic oil using hydroxide-based ionic liquids, Energy Fuels. 29 (2014) 106-111.

[13] R.A. Najmuddin, M.I.A. Mutalib, S.N. Shah, H. Suleman, K.C. Lethesh, R.B.M. Pilus, A.S. Maulud, Liquid-Liquid Extraction of Naphthenic Acid Using Thiocyanate Based Ionic Liquids, Procedia Eng. 148 (2016) 662–670.

[14] R. Lü, C. Wu, J. Lin, Y. Xiao, F. Wang, Y. Lu, The study on interactions between 1-ethyl-

3-methylimidazolium chloride and benzene/pyridine /pyrrole/thiophene, J. Phys. Org. Chem. (2016) 1–7.

[15] I. Khan, K.A. Kurnia, F. Mutelet, S.P. Pinho, J. a P. Coutinho, Probing the Interactions between Ionic Liquids and Water : Experimental and Quantum Chemical Approach Probing the Interactions between Ionic Liquids and Water : Experimental and Quantum Chemical Approach, J. Phys. Chem. B. 118 (2014) 1848–1860.

[16] M. Babucci, V. Balci, A. Akçay, A. Uzun, Interactions of [BMIM][BF_4] with Metal Oxides and Their Consequences on Stability Limits, J. Phys. Chem. C. 120 (2016) 20089–20102.

[17] P. Verdía, E.J. González, D. Moreno, J. Palomar, E. Tojo, Deepening of the Role of Cation Substituents on the Extractive Ability of Pyridinium Ionic Liquids of N-Compounds from Fuels, ACS Sustain. Chem. Eng. 5 (2017) 2015–2025.

[18] E. Kianpour, S. Azizian, M. Yarie, M.A. Zolfigol, M. Bayat, A task-specific phosphonium ionic liquid as an efficient extractant for green desulfurization of liquid fuel: An experimental and computational study, Chem. Eng. J. 295 (2016) 500–508.

[19] M.H. Ibrahim, M. Hayyan, M.A. Hashim, A. Hayyan, The role of ionic liquids in desulfurization of fuels: A review, Renew. Sustain. Energy Rev. 76 (2015) 1534–1549.

[20] M.J. Frisch, *et al.* Gaussian 09, Revision E.01, Gaussian, Inc., Wallingford CT, 2009.

[21] A. Liu, R. Ma, C. Song, Z. Yang, A. Yu, Y. Cai, L. He, N. Zhao, B. Yu, Q. Song, Equimolar CO_2 Capture by N-Substituted Amino Acid Salts and Subsequent Conversion, Angew. Chemie Int. Ed. 51 (2012) 11306–11310.

[22] A.M. Socha, R. Parthasarathi, J. Shi, S. Pattathil, D. Whyte, Efficient biomass pretreatment using ionic liquids derived from lignin and hemicellulose, Proc. Natl. Acad. Sci. 111 (2014) 3587–3595.

[23] N. Sun, R. Parthasarathi, A.M. Socha, J. Shi, S. Zhang, V. Stavila, K.L. Sale, B.A. Simmons, S. Singh, Understanding pretreatment efficacy of four cholinium and imidazolium ionic liquids by chemistry and computation, Green Chem. 16 (2014) 2546–2557.

[24] B.A. Marekha, O.N. Kalugin, A. Idrissi, Non-covalent interactions in ionic liquid ion pairs and ion pair dimers : a quantum chemical calculation analysis, Phys. Chem. Chem. Phys. 17 (2015) 16846–16857.

[25] C. Allen, R. Ghebreab, B. Doherty, B. Li, O. Acevedo, Examining Ionic Liquid E ff ects on Mononuclear Rearrangement of Heterocycles Using QM/MM Simulations, J. Phys. Chem. B. 120 (2016). 10786-10796.

[26] T. Lu, F. Chen, Multiwfn: A multifunctional wavefunction analyzer, J. Comput. Chem. 33 (2012) 580–592.

[27] T. Lu, F. Chen, Quantitative analysis of molecular surface based on improved Marching Tetrahedra algorithm, J. Mol. Graph. Model. 38 (2012) 314–323.

[28] J. Yang, X. Wang, W. Yim, Q. Wang, Computational Study on the Intramolecular Charge Separation of D⁻A-π⁻A Organic Sensitizers with Different Linker Groups, J. Phys. Chem. C. 119 (2015) 26355–26361.

[29] R.F.W. Bader, A quantum theory of molecular structure and its applications, Chem. Rev. 91 (1991) 893–928.

[30] N.A. Wazzan, O.S. Al-qurashi, H.M. Faidallah, DFT/and TD-DFT/PCM calculations of molecular structure, spectroscopic characterization, NLO and NBO analyses of 4-(4-chlorophenyl) and 4-[4-(dimethylamino) phenyl]-2-oxo-1, 2, 5, 6-tetrahydrobenzo[h] quinoline-3-carbonitrile dyes., J. Mol. Liq. 223 (2016) 29–47.

[31] A. Bondi, van der Waals Volumes and Radii, J. Phys. Chem. 68 (1964) 441–451.

[32] L. Chęcińska, S.J. Grabowski, M. Małecka, An analysis of bifurcated H-bonds: Crystal and molecular structures of O,O-diphenyl 1-(3-phenylthioureido) pentanephosphonate and O,O-diphenyl 1-(3-phenylthioureido)butanephosphonate, J. Phys. Org. Chem. 16 (2003) 213–219.

[33] R.F.W. Bader, A bond path: a universal indicator of bonded interactions, J. Phys. Chem. A. 102 (1998) 7314–7323.

[34] S. Casassa, A. Erba, J. Baima, R. Orlando, Electron density analysis of large (molecular and periodic) systems: A parallel implementation, J. Comput. Chem. 36 (2015) 1940–1946.

[35] E.R. Johnson, S. Keinan, P. Mori-Sánchez, J. Contreras-García, A.J. Cohen, W. Yang, Revealing noncovalent interactions, J. Am. Chem. Soc. 132 (2010) 6498–6506.

[36] A.S. Ogunlaja, E. Hosten, Z.R. Tshentu, Dispersion of Asphaltenes in Petroleum with Ionic Liquids: Evaluation of Molecular Interactions in the Binary Mixture, Ind. Eng. Chem. Res. 53 (2014) 18390–18401.

[37] T.G.A. Youngs, C. Hardacre, Application of static charge transfer within an ionic-liquid force field and its effect on structure and dynamics, ChemPhysChem. 9 (2008) 1548–1558.

[38] K. Noack, P.S. Schulz, N. Paape, J. Kiefer, P. Wasserscheid, A. Leipertz, The role of the C2 position in interionic interactions of imidazolium based ionic liquids: a vibrational and NMR spectroscopic study, Phys. Chem. Chem. Phys. 12 (2010) 14153.

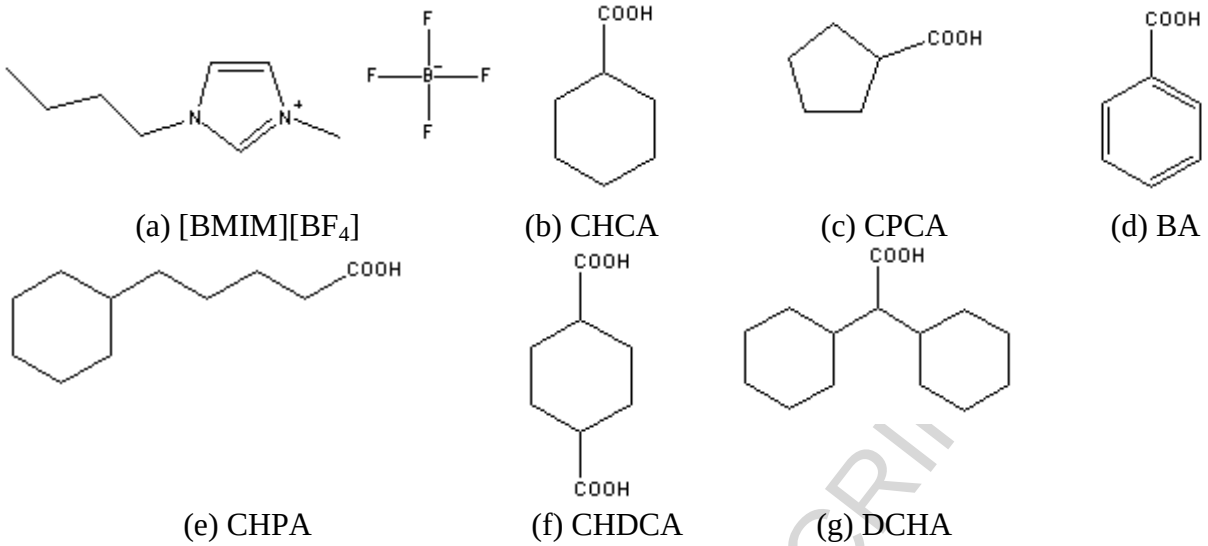

(a) [BMIM][BF_4] (b) CHCA (c) CPCA (d) BA

(e) CHPA (f) CHDCA (g) DCHA

Fig. 1. Structures of [BMIM][BF_4] and six types of model NAs compounds.

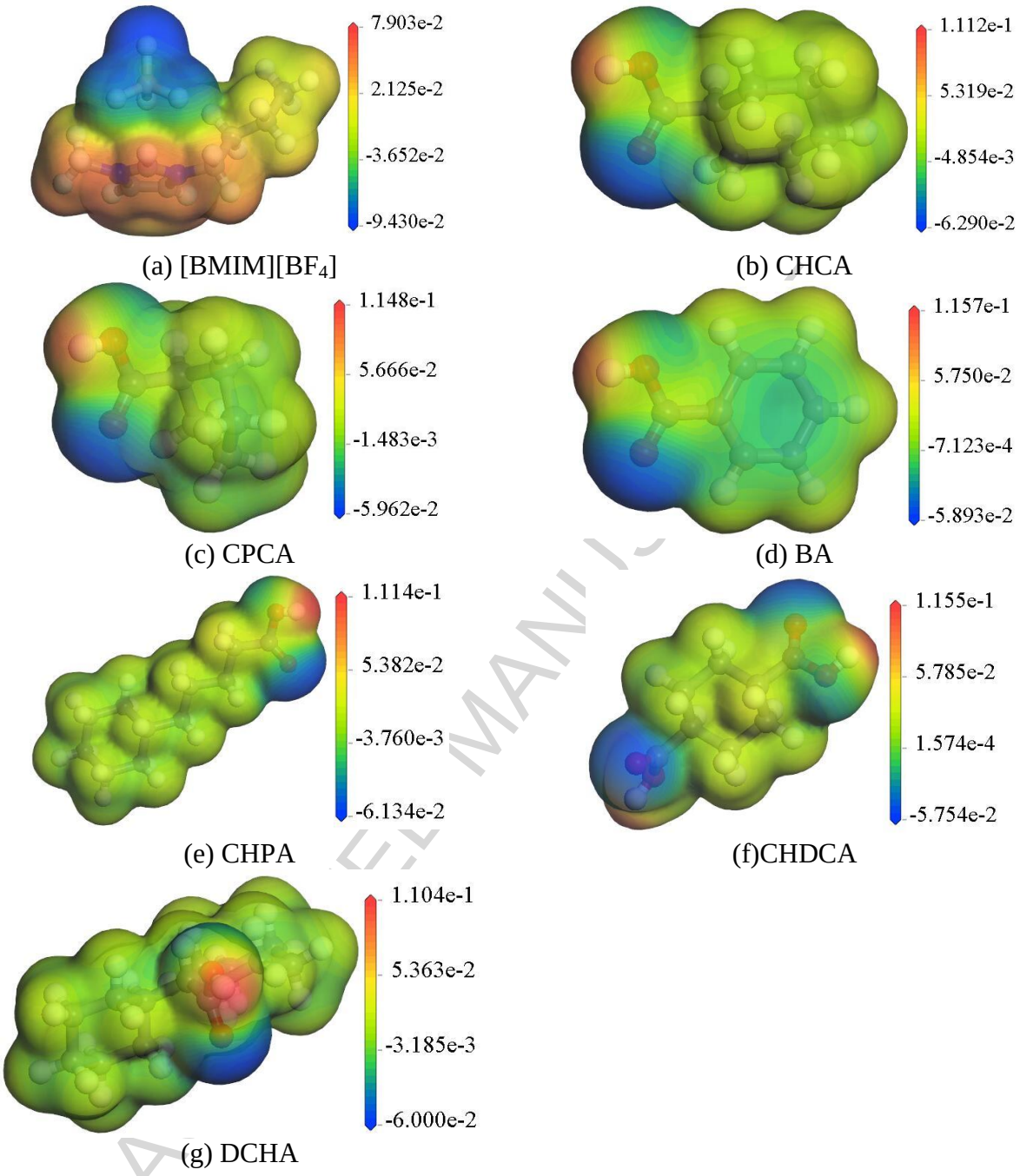

Fig. 2. The electrostatic potential (a.u.) of (a) [BMIM][BF_4], (b) CHCA, (c) CPCA , (d) BA, (e) CHPA, (f) CHDCA, and (g) DCHA.

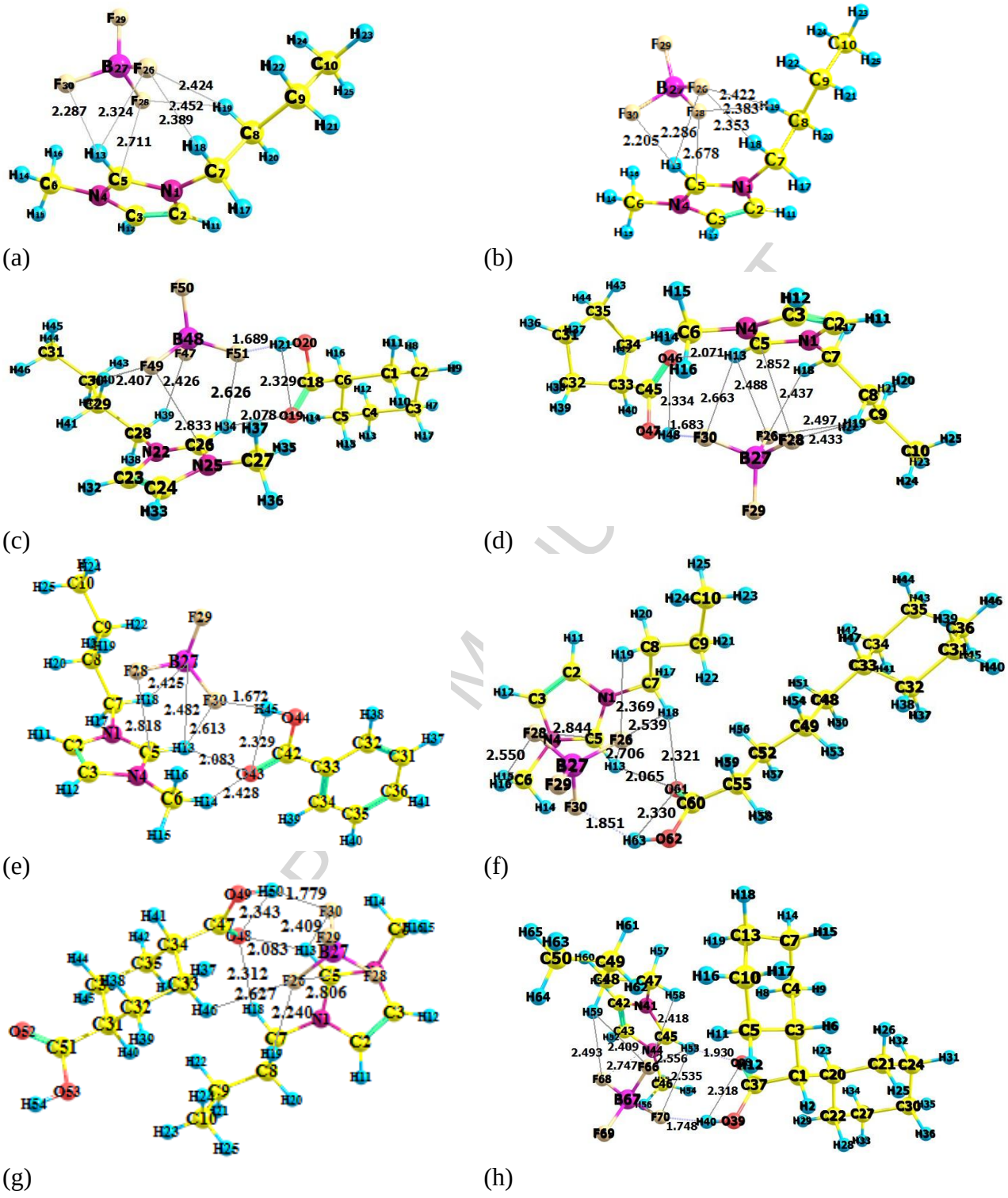

Fig. 3. The optimized structures of (a) [BMIM][BF_4] calculated by 6-311++G(d,p) basis set, (b) [BMIM][BF_4] calculated by 6-311G(d,p) basis set, (c) [BMIM][BF_4]-CHCA, (d) [BMIM][BF_4]-CPCA, (e) [BMIM][BF_4]-BA, (f) [BMIM][BF_4]-CHPA, (g) [BMIM][BF_4]-CHDCA, and (h) [BMIM][BF_4]-DCHA.

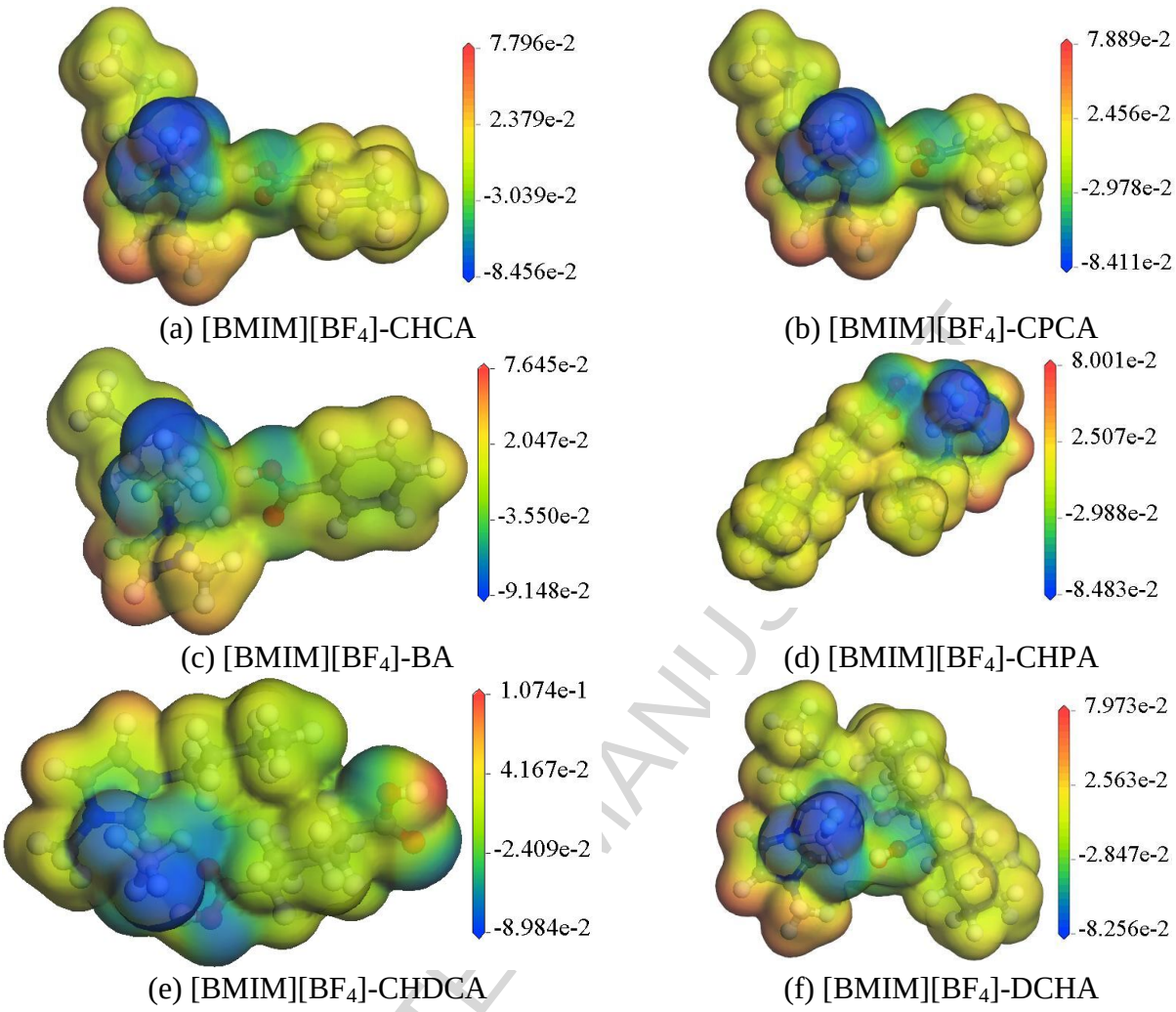

Fig. 4. The electrostatic potential (a.u.) of (a) [BMIM][BF_4]-CHCA, (b) [BMIM][BF_4]-CPCA , (c) [BMIM][BF_4]-BA, (d) [BMIM][BF_4]-CHPA, (e) [BMIM][BF_4]-CHDCA, and (f) [BMIM][BF_4]-DCHA.

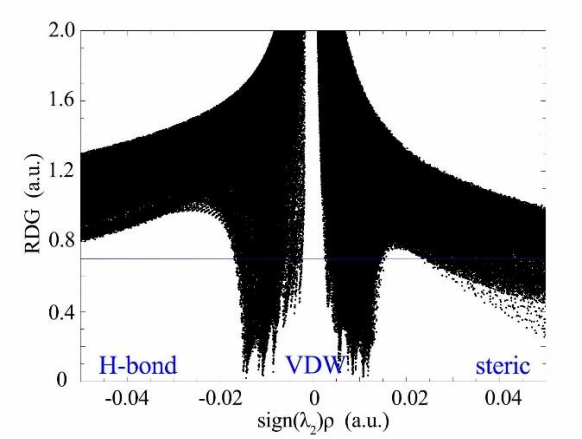

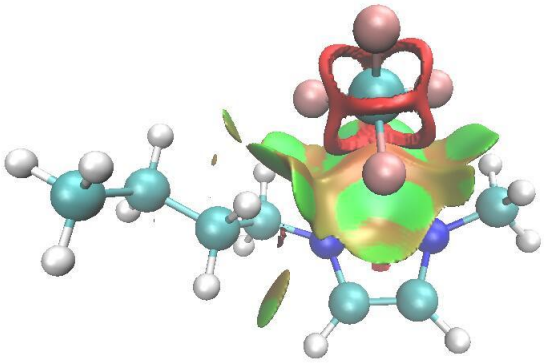

(a)

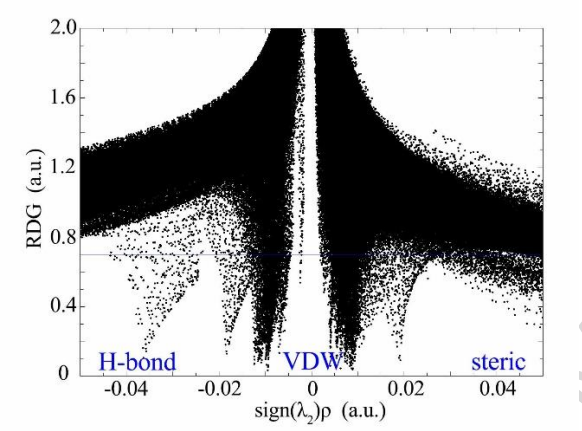

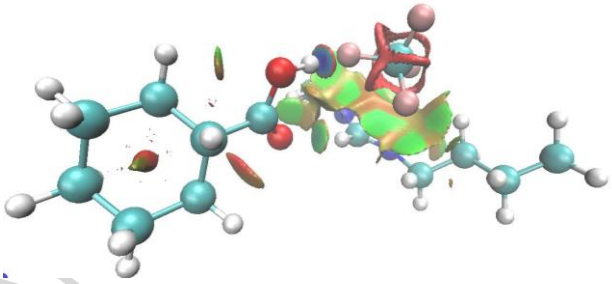

(b)

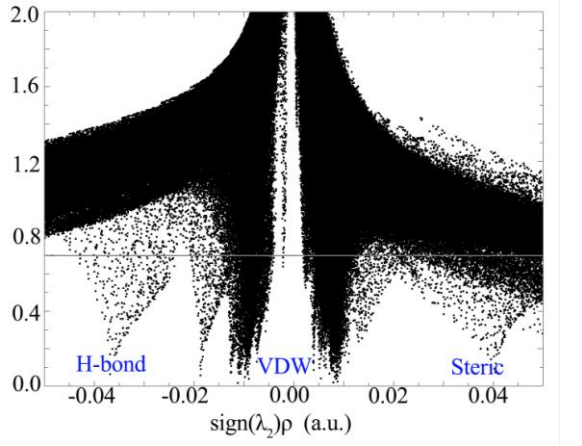

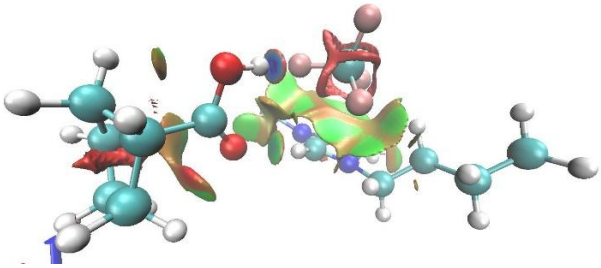

(c)

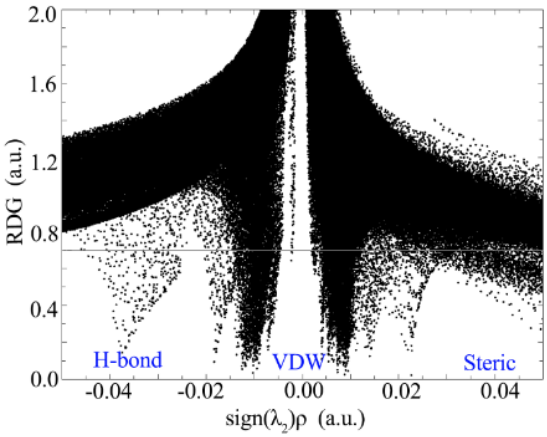

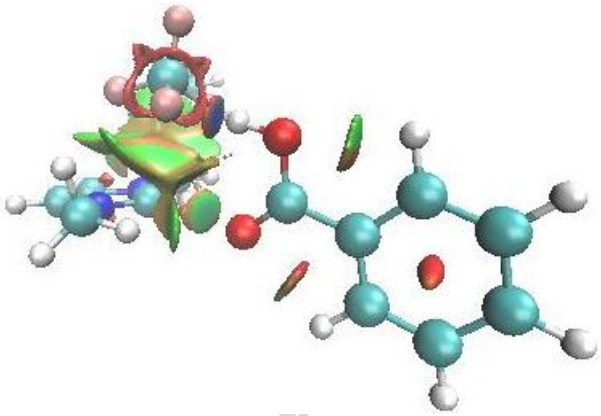

(d)

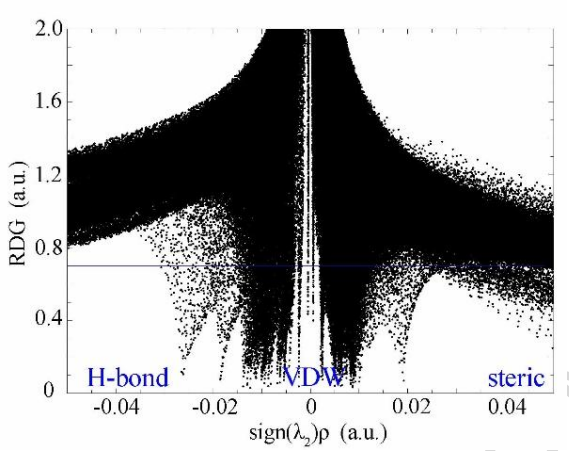

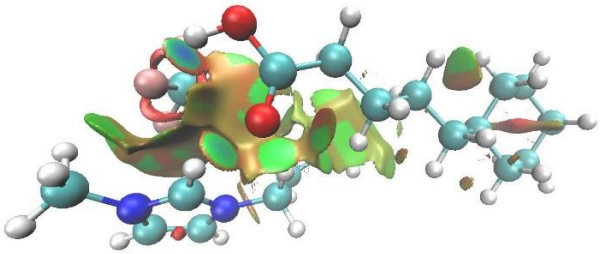

(e)

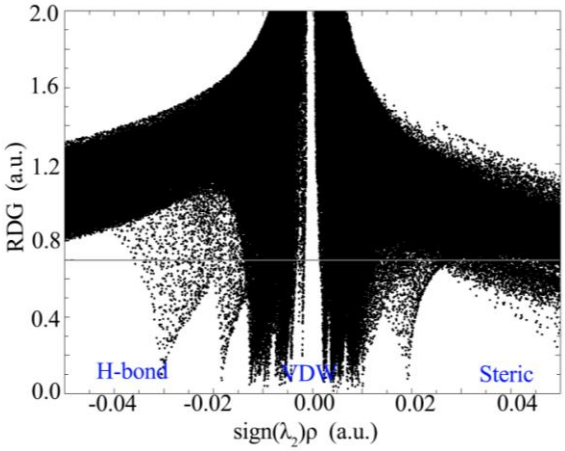

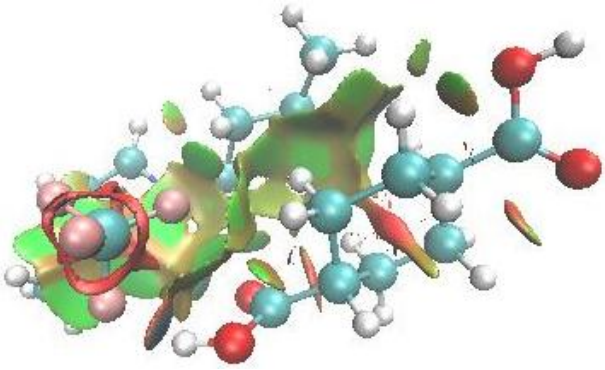

(f)

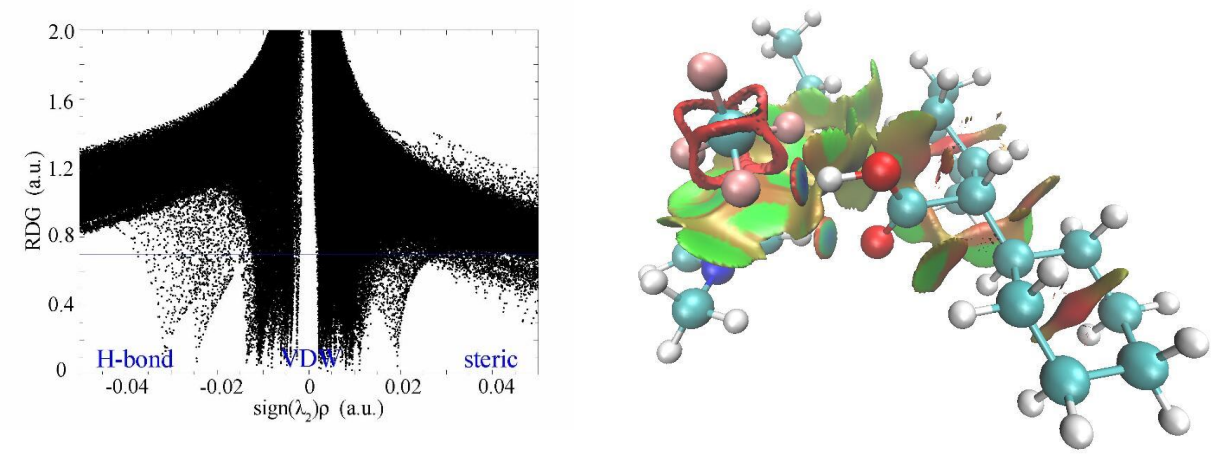

(g)

Fig. 5. The sign(λ_2)ρ vs RDG (left) and the gradient isosurfaces (right) for (a) [BMIM][BF_4], (b) [BMIM][BF_4]-CHCA, (c) [BMIM][BF_4]-CPCA , (d) [BMIM][BF_4]-BA, (e) [BMIM][BF_4]-CHPA, (f) [BMIM][BF_4]-CHDCA, and (g) [BMIM][BF_4]-DCHA. Note: red indicated sign(λ_2)ρ >0, blue indicated sign(λ_2)ρ <0

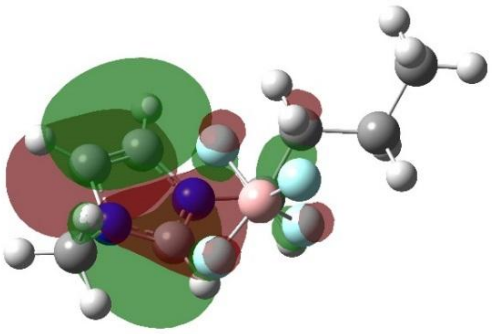

[BMIM][BF_4] HOMO

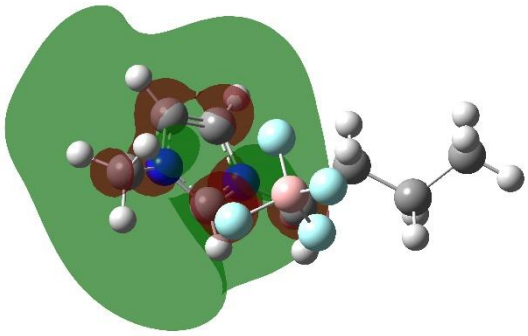

[BMIM][BF_4] LUMO

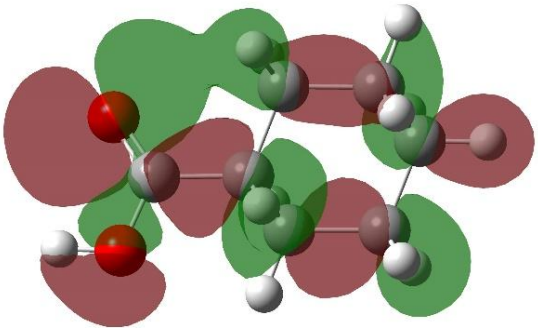

CHCA HOMO

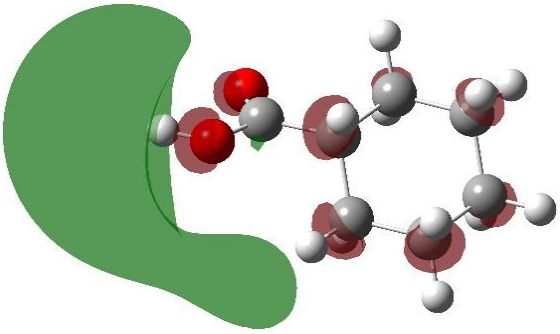

CHCA LUMO

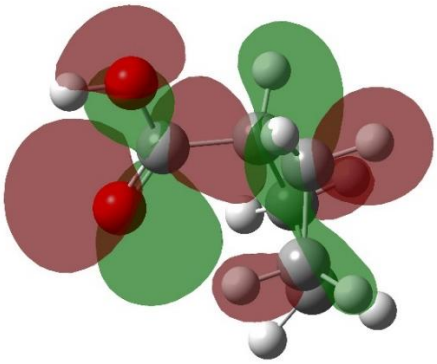

CPCA HOMO

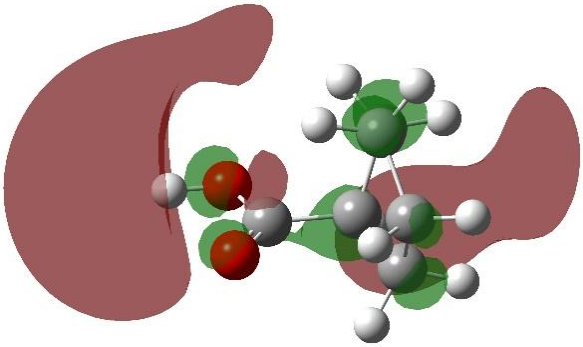

CPCA LUMO

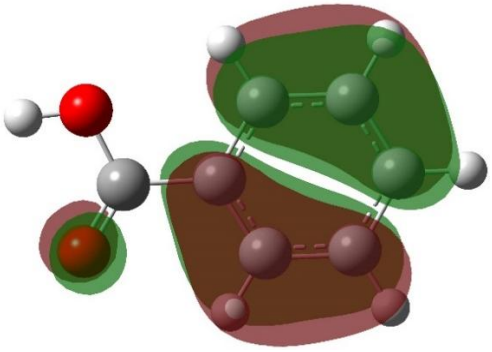

BA HOMO

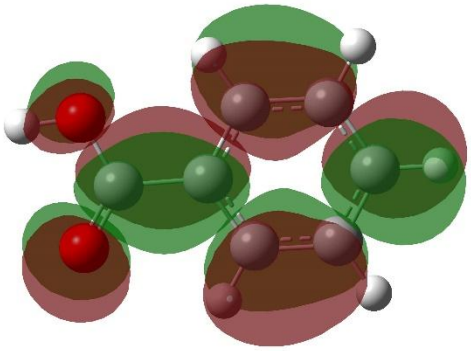

BA LUMO

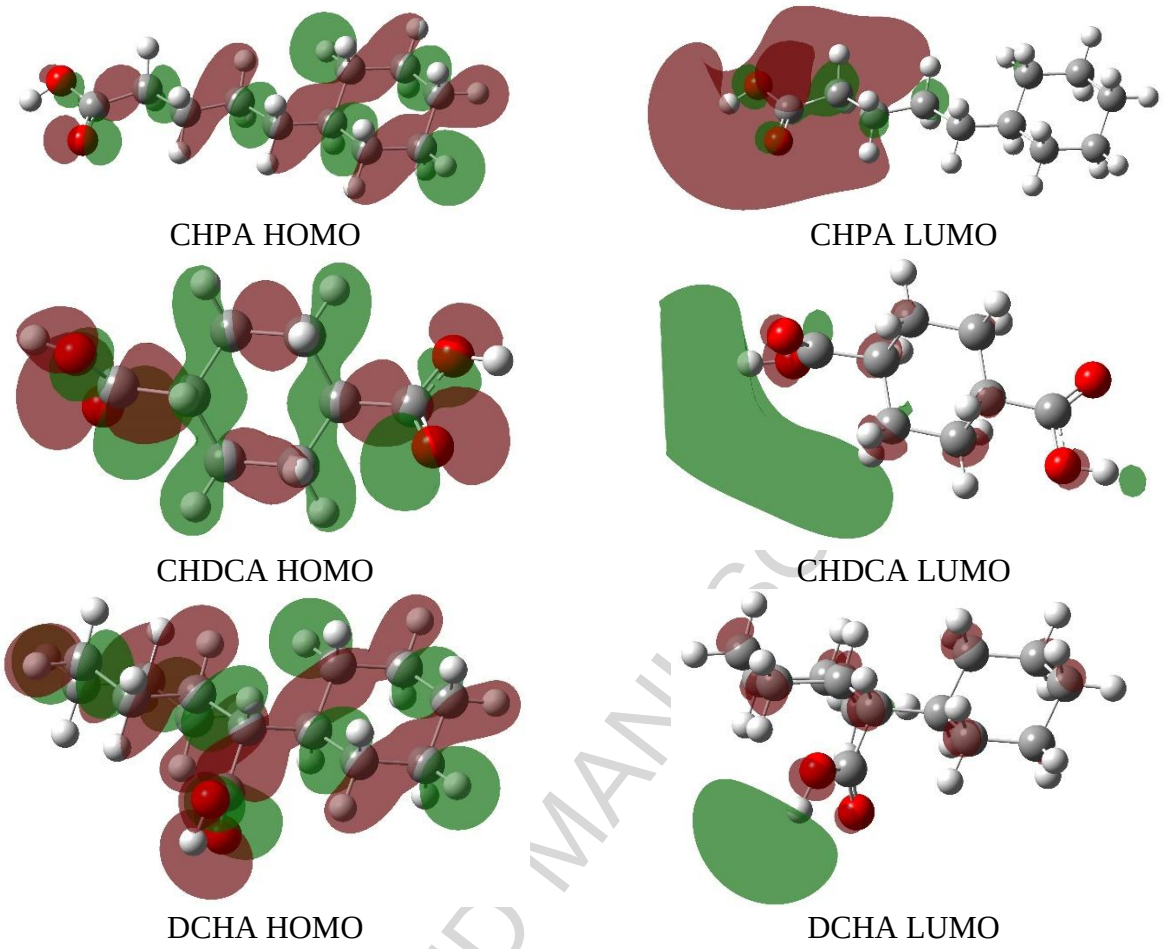

Fig. 6. HOMO LUMO analysis of [BMIM][BF_4] and model NAs. Note: isosurface for CHDCA LUMO is at 0.021 a.u., CHPA LUMO is at 0.022 a.u., and the others is 0.02 a.u.; green represent negative values, dark red represents positive values.

Graphical abstract

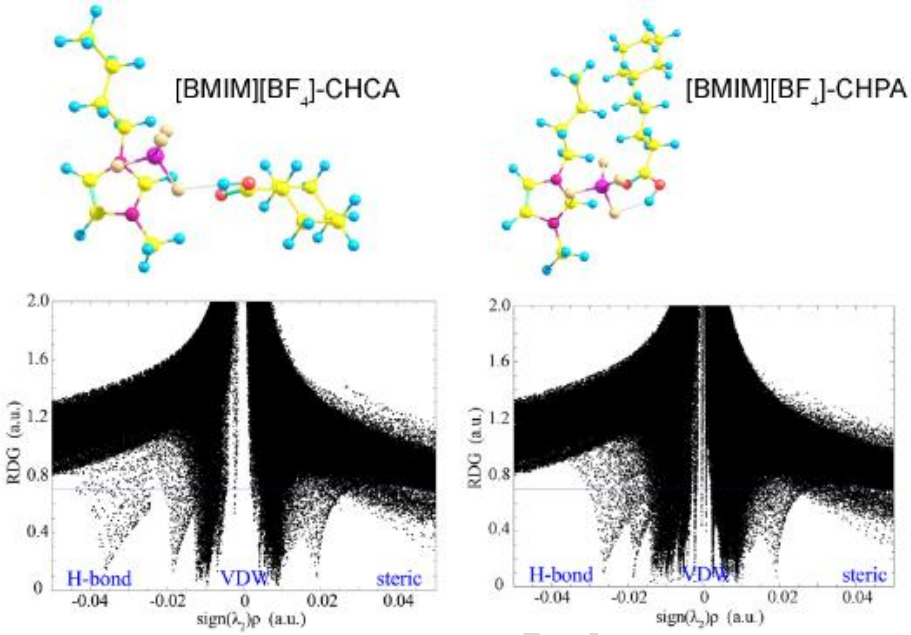

Highlights

- Ionic liquids offer an effective method to remove naphthenic acids from crude oil
- Explored interactions between ([BMIM][BF_4]) and model naphthenic acids
- Hydrogen bonding is main extraction mechanism for NAs without long alkyl chain
- VdW interaction and H bonding dominant extraction mechanisms for alkyl chain NAs
- Electron density changes near $[BF_4]^-$ and carboxylic group upon complex formation